Neural excitability increases with axonal resistance between soma and axon initial segment

Aurélie Fékété[a] , Norbert Ankri[a] , Romain Brette[b,1] , and Dominique Debanne[a,1]

[a]UMR 1072, INSERM, Unité de Neurobiologie des canaux Ioniques et de la Synapse, Aix-Marseille Université, 13015 Marseille, France; and [b]INSERM, CNRS, Institut de la Vision, Sorbonne Université, 75012 Paris, France

The position of the axon initial segment (AIS) is thought to play a critical role in neuronal excitability. Previous experimental studies have found that a distal shift in AIS position correlates with a reduction in excitability. Yet theoretical work has suggested the opposite, because of increased electrical isolation. A distal shift in AIS position corresponds to an elevation of axial resistance R_a. We therefore examined how changes in R_a at the axon hillock impact the voltage threshold (V_{th}) of the somatic action potential in L5 pyramidal neurons. Increasing R_a by mechanically pinching the axon between the soma and the AIS was found to lower V_{th} by $\sim$6 mV. Conversely, decreasing R_a by substituting internal ions with higher mobility elevated V_{th}. All R_a-dependent changes in V_{th} could be reproduced in a Hodgkin–Huxley compartmental model. We conclude that in L5 pyramidal neurons, excitability increases with axial resistance and therefore with a distal shift of the AIS.

neuronal excitability | sodium current | action potential | axon | plasticity

In most vertebrate neurons, the action potential (AP) is initiated in the axon initial segment (AIS), a few tens of micrometers away from the soma (1, 2). Several studies have found that inducing a distal shift of the AIS is accompanied with a reduction of excitability (3–5). However, these changes in excitability could be due to confounding factors (6), such as the phosphorylation of voltage-gated sodium (Nav) channels (7) or regulation of Kv channels (8–10). In pyramidal neurons, observational studies found no (11) or the opposite (12) correlation between AIS position and excitability. Disentangling the various potential factors is experimentally challenging.

In theory, a distal shift of the AIS could increase the electrical isolation of the AIS, resulting in greater excitability (13). Specifically, resistive coupling theory (14–16) predicts that the spike threshold varies as $-k_a log(R_a)$, where k_a is the activation slope of Nav channels, and R_a is the axial resistance between the soma and the middle of the AIS. The axial resistance of an axon of length x and uniform section area S is $R_a = R_i x/S$, where R_i is intrinsic resistivity (100 to 150 Ω.cm); thus, to a first approximation, R_a is proportional to the distance of the AIS. Briefly, the above relation between R_a and the threshold comes from the fact that, at spike initiation, the Na$^+$ current at the AIS, proportional to e^{V/k_a}, must match the resistive current flowing toward the soma, which by Ohm's law is proportional to $1/R_a$ (14).

However, numerical studies have also occasionally reported an opposite relation, depending on model parameters (3, 4, 17). Theoretically, this can happen if the conditions of resistive coupling are not met, mainly the large capacitance mismatch between the somatodendritic compartment and the axon, or if the AIS is strongly hyperpolarized relative to the soma (15).

We therefore attempted to specifically manipulate the axial resistance R_a of L5 pyramidal neurons, thereby changing the electrotonic distance between the soma and AIS, and we assessed the impact on the voltage threshold (V_{th}) of the somatic AP. We found that increasing R_a by mechanically pinching the axon between the soma and the AIS lowered the spike threshold by $\sim$6 mV. Conversely, reducing R_a by replacing a weakly mobile ion

(gluconate) by a highly mobile ion (chloride) elevated the spike threshold by $\sim$2 mV. All R_a-dependent changes in spike threshold could be reproduced in a Hodgkin–Huxley compartmental model. These data indicate that the spike threshold of L5 pyramidal neurons is inversely related to the axial resistance R_a between the soma and AIS, in agreement with resistive coupling theory. Thus, our results suggest that, contrary to previous suggestions, a distal shift in the AIS position along the axon would result in elevated excitation.

Results

Elevating R_a by Axon Pinching Lowers Spike Threshold. L5 pyramidal neurons were recorded in a whole-cell configuration of the patch clamp technique with a pipette filled with Alexa 488 to visualize the axon. Only neurons having an axon emerging from the cell body were used in this study (11, 12). To test the effects of elevated axial resistance, the pre-AIS region of the axon was pinched with the help of two glass microelectrodes positioned on each side of the axon. In most of the cases, pinching left the axon intact, but a reduction of the transversal section of the axon was observed as a drop of Alexa 488 fluorescence where the pinching occurred (*SI Appendix*, Fig. S1). The local fluorescence signal is approximately proportional to the section area, and therefore, the local axial resistance is expected to change with the inverse of the signal.

To ensure that the AIS was intact, only cells with an axonal length greater than 100 μm were selected. Additionally, to rule out potential effects of mechanosensitivity and axonal damage, we excluded all cells in which the holding current changed by more than 70 pA after pinching.

Significance

Action potentials initiate in the axon initial segment (AIS), close to the soma. Previous experimental findings suggested that a distal shift in AIS position reduces excitability, but theoretical work predicts the opposite. A distal shift in AIS position corresponds to an elevation of axial resistance (R_a) between soma and AIS. We modified R_a and measured the voltage threshold (V_{th}) of action potentials in the soma of cortical neurons. Increasing R_a by mechanically pinching the axon hillock lowered V_{th} by $\sim$6 mV, whereas decreasing R_a by substituting internal ions with higher mobility elevated V_{th}. Thus, excitability increases with axial resistance and therefore with a distal shift of the AIS.

NEUROSCIENCE

To minimize the potential effect of Nav channel inactivation, the spike threshold was measured with a fixed initial potential and constant spike latency. Axon pinching led to a significant change in spike threshold in half of the cases (7/14 cases, comparison of spike threshold at constant latency over 10 trials before versus after pinching, Mann–Whitney U test, $P < 0.001$; Fig. 1 A–C and *SI Appendix*, Fig. S2A). The reduction in fluorescence signal at the pinching site was larger in those cells than in cells with nonsignificant threshold change (mean: $79 \pm 6\%$ versus $38 \pm 9\%$; $P < 0.01$, Mann–Whitney U test; *SI Appendix*, Fig. S2B), which suggests that cells with significant threshold change were more efficiently pinched. In all the significant cases, the spike threshold was hyperpolarized by about -6 mV (mean: -5.6 ± 1.6 mV, $n = 7$), up to ~ 10 mV in three cells (Fig. 1C). In one instance, we were able to release the axon and to measure the threshold again, which depolarized (*SI Appendix*, Fig. S2C). The hyperpolarization of the spike threshold was associated with a reduction in the magnitude of the injected current pulse required to maintain a spike latency constant (from 617 ± 74 to 399 ± 74 pA, $n = 7$, Wilcoxon test, $P < 0.05$; mean reduction: -217 ± 72 pA; Fig. 1D), denoting an increase in neuronal excitability. In fact, changes in spike threshold were

linearly correlated with changes in the current step amplitude ($R^2 = 0.96$, $P < 0.001$; Fig. 1D). These effects were related neither to the pinching location nor the axonal length (*SI Appendix*, Fig. S3). No significant variation in resting membrane potential, holding current, input resistance, or latency induced by pinching was observed between the group exhibiting a significant hyperpolarization of the spike threshold and that exhibiting no change in spike threshold (*SI Appendix*, Fig. S3). Taken together, these results indicate that increasing R_a increases neural excitability by hyperpolarizing the AP threshold measured in the cell body in agreement with theory.

Dissociation of Initial Segment and Somatodendritic Components. Theoretical work predicts that the backpropagated current corresponding to the initial segment (IS) component varies inversely with R_a (12, 18). Thus, during pinching, the current may not be sufficient to trigger a full spike (19).

In one cell exhibiting a significant hyperpolarization of the spike threshold, the amplitude of the AP evoked during pinching was found to be considerably reduced in amplitude (Fig. 2 A and B). The presence of this spikelet was not due to any damage caused to the neuron. In fact, a full spike could be recovered
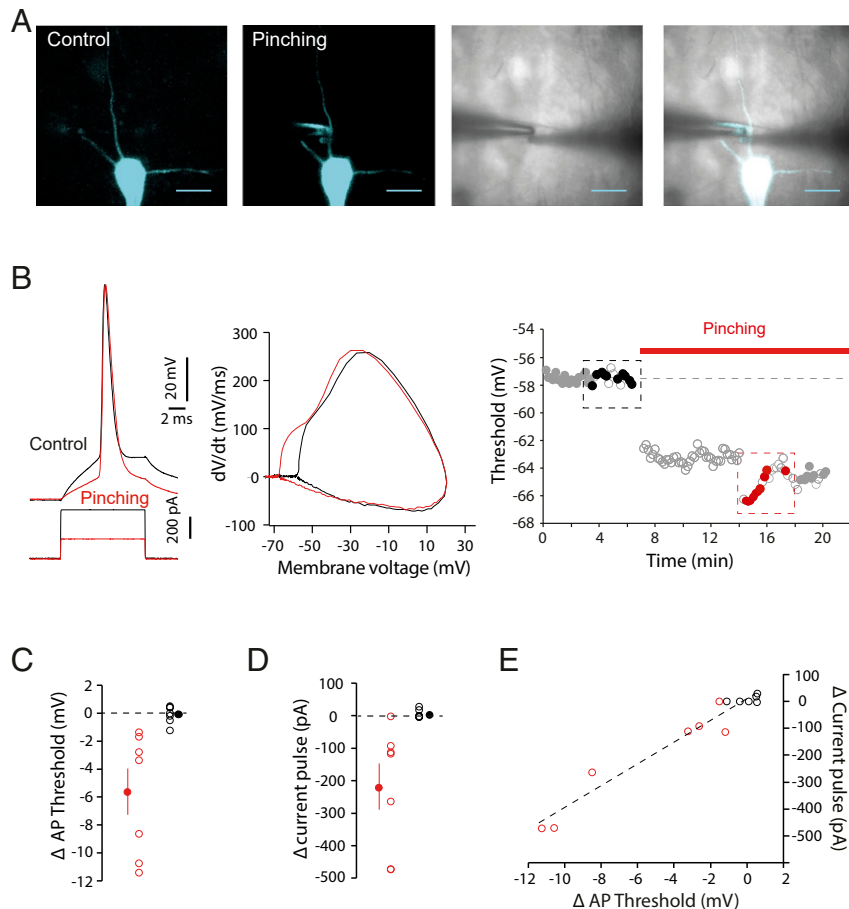

Fig. 1. Axon pinching lowers spike threshold. (*A*) Confocal and infrared images of the neuron filled with Alexa 488, and imaged before and during axon pinching. (Calibration bar: 20 μm.) (*B*) Hyperpolarization of the spike threshold during pinching. (*Left*) Voltage traces (black, before, and red, during pinching). (*Middle*) Phase plots. (*Right*) Time course of the spike threshold. The effect of pinching on the spike threshold was tested using 10 trials before and during pinching at fixed V$_m$ and fixed spike latency (these data are represented in black for the control and in red for the test). The data illustrated as empty gray circles correspond to data that do not meet the selection criteria either because of a deviation in membrane potential larger than 1 mV or because of latency variation greater than 1 ms (data in the time period from 7 to 14 min). Here, a significant difference was found between the two samples (Mann–Whitney U, $P < 0.001$). (*C*) Variation in AP threshold. Neurons showing a significant effect are in red, whereas those showing a nonsignificant effect are in black. Means are represented by filled circles. (*D*) Variation in the current pulse amplitude used to elicit an AP at constant latency. (*E*) Variations in AP threshold were positively correlated with variations in current pulse amplitude ($y = (40.62 \text{ pA/mV}).x + 8.07 \text{ pA}$; $R^2 = 0.95$).
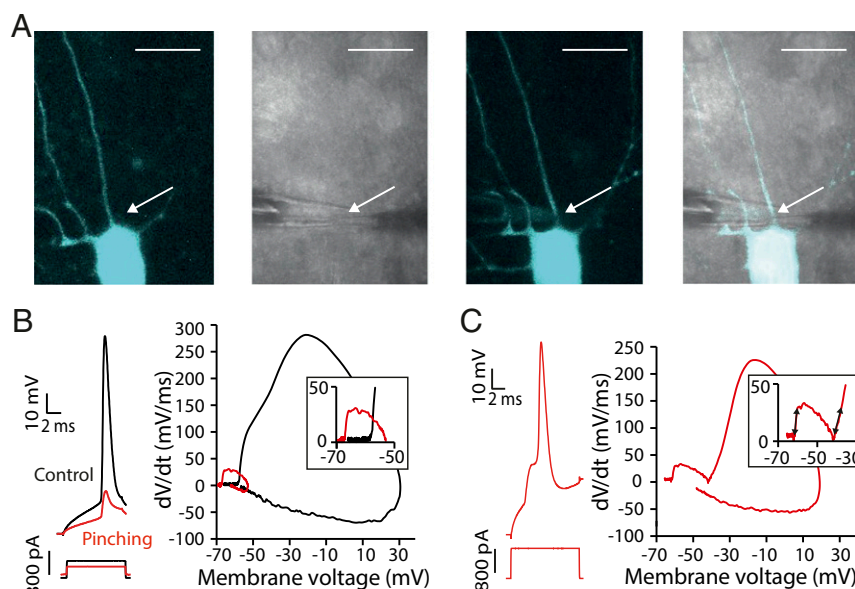
Fig. 2. Dissociation of IS from SD component during axon pinching. (*A*) Confocal and infrared images of the neuron before and during axon pinching. (Calibration bar: 20 μm.) (*B*) During pinching, the spike is hyperpolarized, and its amplitude is considerably reduced. The phase plot shows that the spikelet corresponds to the isolated IS component. (*C*) Increasing current amplitude allows recovery of the full spike amplitude corresponding to the SD component. Note the difference in phase slope for the IS component and the SD component in *Inset*.

when the magnitude of the current step was increased (Fig. 2*C*). This AP was found to exhibit two different phases clearly visible on the phase plot and identified as the IS component and somatodendritic (SD) component (Fig. 2*C*). Interestingly, the slope of the SD component of the AP near the threshold was found to be much slower (6 ms^{-1}) compared to the slope of the IS component (21 ms^{-1}), suggesting that increasing R_a reveals the dissociation of the IS component (fast event) from the SD component (slower event) of the AP.

In three other cases, pinching of the axon accidentally led to an ablation of the axon upstream the AIS. This cut was identified by the abrupt interruption of the intra-axonal fluorescence, disappearance of the IS component on the phase plot of the AP, and depolarization of the spike threshold by ∼8 mV (from −59.1 ±

0.6 versus −51.2 ± 2.3 mV; Fig. 3). Interestingly, onset rapidness was lower after the removal of the AIS (from 37 ± 3 to 14 ± 8 ms^{-1} Fig. 3*C*), indicating that the AP was indeed initiated in the soma rather than in the axon.

Lowering R_a by Intracellular Ion Substitution Elevates Spike Threshold. To further demonstrate that the spike threshold is inversely related to R_a, we decreased the intracellular resistivity by replacing a poorly mobile ion (gluconate) by a highly mobile ion (chloride). For this purpose, L5 pyramidal neurons were recorded sequentially with two intracellular solutions of different composition: solution 1, a gluconate-based solution ([KGlu] = 115 mM and [KCl] = 20 mM), and solution 2, a chloride-based solution ([KGlu] = 0 mM and [KCl] = 135 mM). Because gluconate ions are
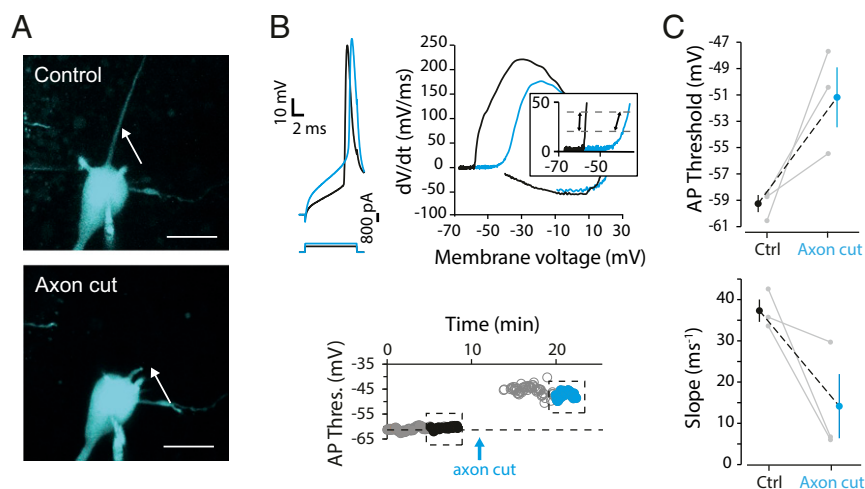

Fig. 3. Cutting the axon upstream the AIS elevates AP threshold. (*A*) Confocal images of the neuron before and after axon cut upstream the AIS. Note the cut axon (*Lower*). (Calibration bar: 20 μm.) (*B*) Depolarization of the AP threshold. (*Top Left*) Voltage traces (black, before, blue, after axon cut). (*Top Right*) Phase plots. Note the difference in the phase slope in each case. (*Bottom*) Time course of AP threshold. The data analyzed in *C* are represented as closed circles (i.e., corresponding to fixed spike delay and constant V_m). (*C*) Group data of changes in AP threshold and onset rapidness before and after axon cut.

www.manaraa.com

about three times less mobile compared to chloride ions (relative mobility of Cl⁻: 1.0388, gluconate ion: 0.33 and K⁺: 1), the total mobility for solution 1 (m_1) is 194 mM, and the total mobility for solution 2 (m_2) is 275 mM.

The predicted change in spike threshold is given by $\Delta\theta = k_a \log \frac{Ra_1}{Ra_2}$. As R_a should be inversely proportional to the total mobility, one predicts that $\Delta\theta = k_a \log \frac{m_2}{m_1}$. With $k_a = 6$ mV, $\Delta\theta = 2.1$ mV (the lower threshold is for the solution with the lower mobility, i.e., solution 1).

We next verified experimentally this theoretical prediction (Fig. 4A). When L5 pyramidal cells were patched with a gluconate-based solution and then repatched with a KCl-based solution, the spike threshold was found to be depolarized in all tested cells ($n = 6$) by ~2 mV on average (1.9 ± 0.6 mV; Wilcoxon test, $P < 0.05$; Fig. 4B). No difference in the magnitude of the current pulse was noted after repatching with KCl-based solution (from 524 ± 74 in K gluconate to 492 ± 71 pA, $n = 6$). Although we cannot exclude inaccuracies in liquid junction potential corrections, the observed elevation in spike threshold agrees quantitatively with the prediction of resistive coupling theory.

Computer Modeling of R_a Change. We reproduced these findings with a compartmental Hodgkin–Huxley model. The model included a cell body, a dendrite, and an axon. When the pre-AIS region was pinched (i.e., modeled as a reduction of the diameter from 2.5 to 0.48 µm in the pre-AIS region corresponding to an increase in R_a from 11 to 50 MΩ between the soma and middle of the AIS, *SI Appendix*, Fig. S4A), the AP threshold was found to be hyperpolarized by ~5 mV (Fig. 5A). The theoretical prediction for this model was $k_a \cdot \log(50/11)$ ~6 mV (14, 15) (*Methods*). Next, we tested the effects of a stronger pinching (corresponding to a further reduction in axon diameter and an elevation in R_a). As expected, a stronger pinching (i.e., corresponding to a reduction of axon diameter to 0.3 µm and an elevation in R_a to 111 MΩ, *SI Appendix*, Fig. S4A) allowed to isolate the IS component of the spike from the SD component (Fig. 5B). As expected, the spike threshold was further hyperpolarized by ~1 mV (Fig. 5 B and D), and the current pulse was reduced (Fig. 5E). Next, we simulated the lowering of R_a by ion substitution with a uniform reduction in R_i by 30% (i.e., the estimated change in resistivity in the experiments). This was found to raise the threshold by ~1.5 mV (Fig. 5 C and D). Thus, the model qualitatively reproduces all the features observed experimentally.

In accordance with theory (12, 18) and previous numerical studies (16), in the model, the rate of rise of the IS component is reduced when the threshold is hyperpolarized (Fig. 5F). In theory, this occurs because the backpropagated current is roughly $\Delta V/R_a$ (by Ohm's law), where $\Delta V \approx E_{Na} - V_{threshold}$ is the voltage gradient between the soma and AIS (12, 18). We verified that this relation was also found in the experimental data. The rate of rise of the IS component was measured on the phase plot at $V_{th} + 5$ mV. A significant correlation was found between the variation in rate of rise of the IS component and the change in

AP threshold ($R^2 = 0.6$, $P < 0.001$; *SI Appendix*, Fig. S4 B and C). This observation further confirms that our experimental manipulations affected the axial resistance.

Discussion

We have shown here that changes in axial resistance in the pre-AIS region of the axon either by axon hillock pinching or by ion substitution changes the AP threshold in L5 pyramidal neurons in the opposite direction. First, pinching the axon hillock was found to hyperpolarize the spike threshold by ~6 mV in half of neurons. Because the efficiency of pinching was only visually controlled, the effect was variable from cell to cell. In the remaining cases, no significant effect was observed on the spike threshold (half of cases). In three neurons, axon pinching led to an elevation of the spike threshold due to axon cut. Second, replacing a weakly mobile ion (gluconate) by a highly mobile ion (chloride) depolarized the spike threshold by ~2 mV. Finally, a Hodgkin–Huxley compartmental model qualitatively reproduced all the effects observed experimentally. In an earlier model of AP initiation in pyramidal cells, the AP threshold was hyperpolarized when intrinsic resistivity increased or diameter decreased, both inducing an increase in axial resistance R_a (20). These data suggest that, contrary to previous hypotheses (3, 4) but in agreement with resistive coupling theory (14–16), the specific effect of a distal displacement of the AIS is an increase in excitability.

Axon Hillock Pinching. When the axon was intact after axon pinching, we found that the AP threshold was hyperpolarized by ~6 mV in a large fraction of the cells. The amplitude of the current that allowed to trigger 1 AP at constant latency was found to be reduced. In fact, the hyperpolarization of the spike threshold was found to be linearly correlated with the reduction of the current pulse. Therefore, the threshold hyperpolarization reflected an increase in excitability rather than a mere change in the properties of the backpropagating AP. Pinching may also have reduced forward transmission from the soma to the AIS. However, this effect must be small since it would imply reduced excitability, the opposite of our observations. Pinching also impacts the backpropagating current as assessed by the reduced rate of rise of the AIS component of the somatic AP (*SI Appendix*, Fig. S4C). This is unlikely to have strongly affected the measurement of somatic threshold because its effect on threshold detection would be in the direction of more depolarized potentials, again the opposite of our observations. Theoretically, the AP threshold measured at the soma reflects the threshold at the AIS with a hyperpolarized shift approximately equal to k_a, the activation slope of Nav channels (14), unless strong non-Na⁺ currents are active at the AIS (15). This is in line with simultaneous patch clamp measurements in the soma and AIS (21).

In one case of pinching, no full spike was recorded in the cell body, but instead a spikelet was triggered by the current pulse. The neuron was not damaged since the holding current was unchanged, and a full spike could still be evoked upon an increase of current step amplitude. Notably, the slope of the phase plot at the
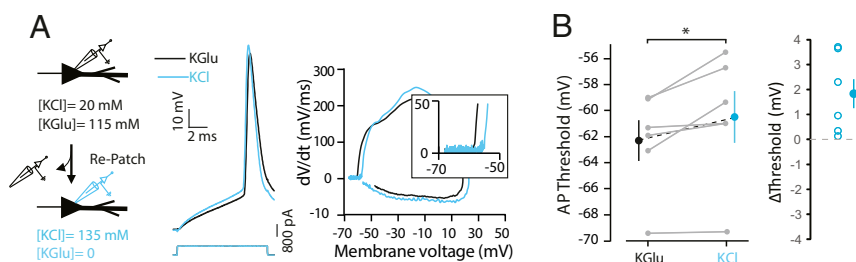

Fig. 4. Lowering R_a by intracellular ion substitution elevates spike threshold. (A) Example of recording a neuron in KGlu and KCl. Note the higher spike threshold on the phase plot. (B) Group data of AP threshold change (*, Wilcoxon, $P < 0.05$).
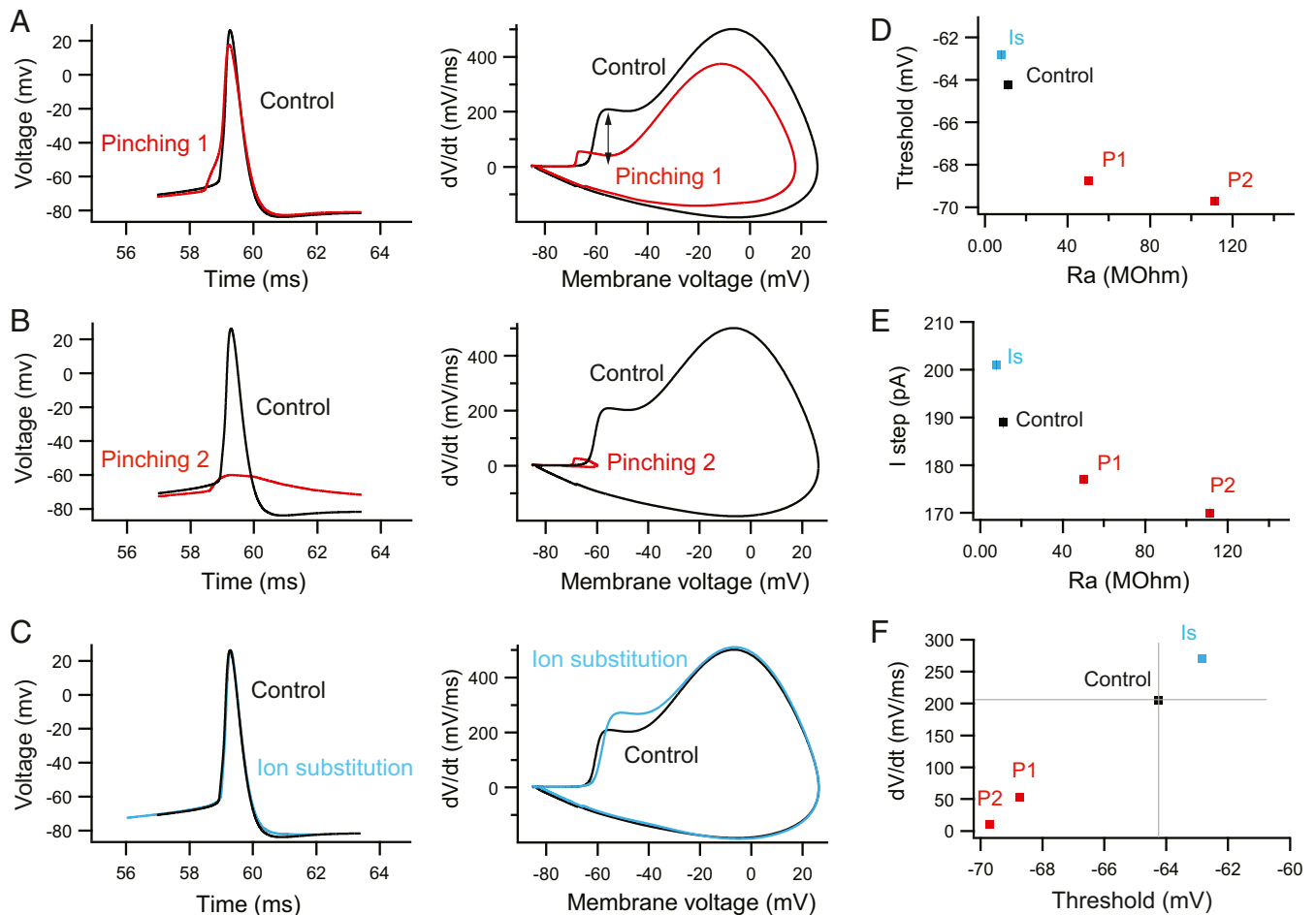
Fig. 5. Computer simulation of R_a change. (*A*) When R_a (taken between the middle of the AIS and the soma) was raised from 11 to 50 MΩ, the spike threshold was found to be hyperpolarized by ~5 mV (see phase plots). (*B*) Raising R_a further to 111 MΩ isolated the IS component (spikelet) and hyperpolarized further the AP threshold (by 1 mV). (*C*) Decreasing intracellular resistivity homogeneously in the neuron to mimic ion substitution raised the spike threshold by ~1.5 mV. (*D*) Plot of AP threshold as a function of R_a. (*E*) Plot of current pulse amplitude as a function of R_a. (*F*) Plot of the first maximum of dV/dt in the IS component as a function of threshold.

spike threshold was found to be much lower for the full spike than for the spikelet, indicating the dissociation of IS and SD components of the AP. These spikelets presumably result from APs that fail to activate sodium channels in the soma (19). This behavior was also observed in the neuron model (Fig. 5). Thus, the scenario of spikelet generation can be reconstituted as follows: axon pinching hyperpolarizes the threshold of the IS spike until a critical value for which the amplitude of the IS spike is too small to activate sodium channels responsible of the SD component, and a spikelet is thus induced.

Axon pinching may have mechanically stimulated Kv1 channels that would promote the opening of these channels (22) or may have triggered depolarizing currents due to calcium channels or to invisible axonal damage. To avoid these potential confounding effects, we excluded cells in which the holding current changed by more than 70 pA after pinching. In addition, we found no difference in holding current between the group exhibiting a significant threshold hyperpolarization and the other one (*SI Appendix*, Fig. S3). Finally, there was no correlation between the change in holding current and the change in threshold. Therefore, the observed change in threshold is unlikely to be due to axonal currents triggered by pinching.

Axon Cut. In a few cases (three cells), axon pinching led to the ablation of the axon at a distance <33 μm, leaving the cell body

isolated from the AIS. Under these conditions, the spike threshold was found to be elevated by ~8 mV, and the spike displayed a smooth onset with no kink. A similar depolarizing shift in the spike threshold has been reported upon the blockade of Nav channels with the local application of tetrodotoxin (TTX) on the AIS (21, 23, 24) or following the genetic disruption of the AIS formation during development (25, 26); in contrast, cutting the axon beyond 30 μm from the soma leaves the threshold essentially unchanged (24). In all cases, only somatic Nav channels are functional. The smooth onset of the spike after an axon cut indicates that after the axon cut, the spike is generated in the cell body.

Ion Substitution. The substitution of gluconate ions by chloride ions was found to elevate the AP threshold by ~2 mV. As this shift is very small, we cannot exclude that it is impacted by inaccuracies in liquid junction potential correction. Unfortunately, it was not possible to decrease resistivity further without breaking osmotic balance. However, we note that the observed value was very close to the value predicted by theory based on ionic mobility. Thus, these data add to the evidence obtained by pinching the axon that excitability is inversely related to AIS proximity (14).

Revisiting the Electrophysiological Impact of AIS Shift. Several studies found that treatments inducing a distal shift of the AIS

also resulted in a lowered excitability in contradiction with our findings (3–5), but observational studies found no such correlation (11, 12). In both types of study, confounding factors could have contributed to excitability changes (6), including the phosphorylation of Nav channels (7) or homeostatic regulation of Kv1 or Kv7 channels (8–10). Modeling studies have also shown mixed results, with either a negative (3) or positive (13, 14) relation between AIS position and excitability or either case depending on model parameters (4, 17). In theory (15), a negative relation between excitability and AIS distance can occur if the conditions of resistive coupling are not met or if the AIS is strongly hyperpolarized relative to the soma—Hu and Bean observed a small hyperpolarization of ~2 mV in L5 pyramidal cells (27). Here, we have tried to alter the electrotonic distance of the AIS specifically in L5 pyramidal cells, and in all cases, we found that an increase in AIS distance was accompanied by an increase in excitability. It remains to be tested whether this relation depends on cell type.

Methods

Acute Slices of Rat Neocortex. Neocortical slices (350 to 400 μm) were obtained from 14- to 20-d-old Wistar rats of both sexes, according to the European and Institutional guidelines (Council Directive 86/609/EEC and French National Research Council and approved by the local health authority, Préfecture des Bouches-du-Rhône, Marseille). Rats were deeply anesthetized with chloral hydrate (intraperitoneal, 200 mg/kg) and euthanized by decapitation. Slices were cut in an ice-cold solution containing (mM) 92 N-methyl-D-glutamine, 30 NaHCO$_3$, 25 D-glucose, 10 MgCl$_2$, 2.5 KCl, 0.5 CaCl$_2$, 1.2 NaH$_2$PO$_4$, 20 Hepes, 5 sodium ascorbate, 2 thiourea, and 3 sodium pyruvate and were bubbled with 95% O$_2$–5% CO$_2$, pH 7.4. Slices were recovered (1 h) in a solution containing 125 NaCl, 26 NaHCO$_3$, 3 CaCl$_2$, 2.5 KCl, 2 MgCl$_2$, 0.8 NaH$_2$PO$_4$, and 10 D-glucose and were equilibrated with 95% O$_2$–5% CO$_2$. Each slice was transferred to a submerged chamber mounted on an upright microscope (Olympus BX51WI or Zeiss Axio Examiner Z1), and neurons were visualized using differential interference contrast infrared videomicroscopy.

Electrophysiological Recordings. Whole-cell recordings from L5 pyramidal neurons were obtained as previously described (28). The external saline contained (in mM) 125 NaCl, 26 NaHCO$_3$, 3 CaCl$_2$, 2.5 KCl, 2 MgCl$_2$, 0.8 NaH$_2$PO$_4$, and 10 D-glucose and was equilibrated with 95% O$_2$–5% CO$_2$. Patch pipettes (5 to 10 MΩ) were pulled from borosilicate glass and filled with an intracellular solution containing (in mM) 115 K gluconate, 20 KCl, 10 Hepes, 0.5 ethylene glycol-bis(β-aminoethyl ether)-N,N,N′,N′-tetraacetic acid (EGTA), 2 MgCl$_2$, 2 Na$_2$ATP, and 0.3 NaGTP (pH = 7.4). In experiments in which the same neuron was repatched with a KCl-containing solution, KCl replaced K gluconate ([K gluconate] = 0 mM and [KCl] = 135 mM). We then let the solution diffuse for 10 min; with a diffusion coefficient of chloride of $D = 2.10^{-5}$ cm^2/s (29), the solution is expected to diffuse by about $\sqrt{2Dt} \approx 1$ mm. Recordings were performed with a MultiClamp 700B (Molecular Devices) at 30 °C in a temperature-controlled recording chamber (Luigs & Neumann). The membrane potential was corrected for the liquid junction potential (−12.2 mV for gluconate-based solution and −2.7 mV for KCl-based solution). Neurons were held at a potential of ~−77 mV. Voltage signals were low-pass filtered (10 kHz), and sequences (200 to 500 ms) were acquired at 50 kHz with pClamp 10 (Axon Instruments, Molecular Devices).

Analyses. Electrophysiological signals were analyzed with ClampFit (Axon Instruments). Pooled data are represented as mean ± SE in all figures, and we used the Mann–Whitney U test or Wilcoxon rank-signed test for statistical comparisons. Spikes were evoked by a short (10 ms) current pulse (300 to 900 pA). As the spike threshold is highly sensitive to sodium channel inactivation (30), the latency of the spike was maintained constant (ΔLat < 1 ms) before and after axon pinching or axon cut. For this purpose, the amplitude of the current step was adjusted. With this methodology, a lower voltage threshold implies a smaller rate of rise, which may contribute a depolarization of the threshold. Therefore, discarding the effect of inactivation would increase the hyperpolarization.

Trials were considered when fluctuations in spike latency were maintained within 1 ms. Only trials for which V$_m$ was comparable before and after pinching (ΔV$_m$ < 1 mV) were kept for final analysis. For each cell, statistical analysis was performed on the 10 last trials in control versus the first 10 trials during pinching.

The AP threshold was determined on the spike phase plot with a custommade software programmed in LabView. The recording noise was reduced by smoothing the phase plot with a polynomial of order 4. Then, the AP threshold was determined in the phase plot as the maximum of the second derivative of dV/dt with respect to voltage (Method II as described in ref. 31).

Axon Pinching and Cutting Under Confocal Imaging. To visualize the morphology of L5 pyramidal neurons, Alexa 488 (50 μM) was added to a pipette solution and was let to diffuse for at least 10 to 15 min before imaging the axon with a confocal microscope (Zeiss; LSM-710) (32). Alexa 488 was excited by a laser source at 488 nm. The axon was identified as a thin, aspiny process emerging from the soma or a proximal dendrite at the basal pole of the neuron. Two electrodes were positioned on each side of the axon. To pinch the axon, the two electrodes were gently moved toward each other (33). The efficacy of pinching was evaluated by visualizing the decrease in fluorescence at the pinched axon. In a few cases, fluorescence was measured with the use of ImageJ (NIH). In a few cases, pinching the axon led to an axon cut at a mean distance of 23 ± 6 μm ($n = 3$) from the soma. In this case, the cut axon was identified by the abrupt disappearance of Alexa fluorescence.

Hodgkin–Huxley Modeling. Computer simulations were performed with LabView 10. The simplified morphology of an L5 pyramidal neuron included dendrite, soma, pre-AIS, AIS, and axon. We did not consider myelination, as it has a small impact on AP initiation (15). Similarly, we chose a uniform channel distribution for simplicity because it has no qualitative impact on the phenomenon (14). The diameter, length, and number of subcompartments in each neuronal element are provided in *SI Appendix*, Table S1. The membrane capacitance (C$_m$) was set to 0.7 μF/cm^2 uniformly throughout all compartments (34). Intracellular resistivity was set to 150 Ω.cm.

The voltage dependence of activation and inactivation of a Hodgkin–Huxley-based conductance model (g_{Na}, g_{Kdr}, g_{Kv1}) are given as follows:

$$g_{Na} = G_{Na} * m^3 * h,$$

$$g_{Kdr} = G_{Kdr} * n, \text{ and}$$

$$g_{Kv1} = G_{Kv1} * p^3 * q,$$

where m, n, and p are dynamic activation variables for Na, Kdr, and Kv1 channels, respectively, and h and q are dynamic inactivation variables for Na current and Kv1 channels, respectively. They evolve according to the following differential equations (35):

for $x = \{m, h, n\}$,

$$dx/dt = \alpha_x(1 - x) - \beta_x x,$$

$$\alpha_m = 0.1(v + 45.03)/(1 - \exp(-(v + 45.03)/9)),$$

$$\beta_m = 0.1(v + 45.03)/(\exp((v + 45.03)/9) - 1),$$

$$\alpha_h = 0.02(-v + 60.03)/(1 - \exp(-(-v - 60.03)/7)),$$

$$\beta_h = 0.02(-v - 60.03)/(\exp((-v - 60.03)/7) - 1),$$

$$\alpha_n = (1/600)(v + 55.04)/(1 - \exp(-(v + 55.04)/10)), \text{ and}$$

$$\beta_n = (1/600)(v + 55.04)/(\exp((v + 55.04)/10) - 1),$$

with v in millivolts and α and β in milliseconds^{-1}.

Table 1. Intracellular resistivity equivalent to axon diameter changes in the pre-AIS region and corresponding axial resistances

D_{eq} (μm)	Resistivity (Ω.cm)	r_a (MΩ)	R_a (MΩ)	I step (pA)*
2.5	150	1.5	11.1	189
0.484	4,000	40.7	50.3	177
0.306	10,000	101.9	111.4	170

r_a: axial resistance per unit length; total R_a: axial resistance between soma and middle of the AIS.

*Current step used to generate a fixed latency AP (refer to Fig. 5E).

www.manaraa.com

For this model, an asymptotic expansion for hyperpolarized voltages ($v \to -\infty$) gives the following exponential scaling for the equilibrium activation variable: $m_\infty(v) \sim e^{v/9}$ mV, and thus, at spike initiation, the sodium current scales with the voltage as $m_\infty^3(v) \sim e^{v/k_a}$ with $k_a = 3$ mV. This allows us to predict the effect of axon pinching according to the formula $V_{\text{threshold}} \sim -k_a \log R_a$ (14, 15).

The Kv1 channel model is taken from (36).

$$dp/dt = (p_\infty - p)/T_p,$$

$$dq/dt = (q_\infty - q)/T_q,$$

$$p_\infty = 1/(1 + \exp(-(v - \theta_p)/\sigma_p)), \text{ and}$$

$$q_\infty = 1/(1 + \exp(-(v - \theta_q)/\sigma_q)),$$

with $\theta_p = -50$ mV, $\sigma_p = 20$ mV, $\tau_p = 2$ ms, $\theta_q = -70$ mV, $\sigma_q = -6$ mV, and $\tau_q = 150$ ms.

The pinching of the axon by two pipettes was simulated as the narrowing of the axon diameter without a change in membrane surface. A piece of axon with a length L, resistivity R_i, and section S has a resistance R given by $R = R_i L/S$. The axial resistance per unit length $r_a = R_i/S$ can be modified equivalently by changing the section S or by changing the resistivity from R_i to R_i' of this element. Thus, changing the diameter from D to D' can be simulated by changing the resistivity from R_i to $R_i' = (D/D')^2$.

For three diameter values of the model, we show in Table 1 the equivalent resistivities and the resulting axial resistances with a reference diameter of 2.5 μm as illustrated in *SI Appendix*, Fig. S4. R_a is measured from the soma to the middle of the AIS.

Data Availability. All study data are included in the article and/or *SI Appendix*.

1. K. J. Bender, L. O. Trussell, The physiology of the axon initial segment. *Annu. Rev. Neurosci.* **35**, 249–265 (2012).
2. D. Debanne, E. Campanac, A. Bialowas, E. Carlier, G. Alcaraz, Axon physiology. *Physiol. Rev.* **91**, 555–602 (2011).
3. M. S. Grubb, J. Burrone, Activity-dependent relocation of the axon initial segment fine-tunes neuronal excitability. *Nature* **465**, 1070–1074 (2010).
4. J. Lezmy *et al.*, M-current inhibition rapidly induces a unique CK2-dependent plasticity of the axon initial segment. *Proc. Natl. Acad. Sci. U.S.A.* **114**, E10234–E10243 (2017).
5. W. Wefelmeyer, D. Cattaert, J. Burrone, Activity-dependent mismatch between axo-axonic synapses and the axon initial segment controls neuronal output. *Proc. Natl. Acad. Sci. U.S.A.* **112**, 9757–9762 (2015).
6. M. H. Kole, R. Brette, The electrical significance of axon location diversity. *Curr. Opin. Neurobiol.* **51**, 52–59 (2018).
7. M. D. Evans, A. S. Dumitrescu, D. L. H. Kruijssen, S. E. Taylor, M. S. Grubb, Rapid modulation of axon initial segment length influences repetitive spike firing. *Cell Rep.* **13**, 1233–1245 (2015).
8. R. H. Cudmore, L. Fronzaroli-Molinieres, P. Giraud, D. Debanne, Spike-time precision and network synchrony are controlled by the homeostatic regulation of the D-type potassium current. *J. Neurosci.* **30**, 12885–12895 (2010).
9. F. Kirchheim, S. Tinnes, C. A. Haas, M. Stegen, J. Wolfart, Regulation of action potential delays via voltage-gated potassium Kv1.1 channels in dentate granule cells during hippocampal epilepsy. *Front. Cell. Neurosci.* **7**, 248 (2013).
10. H. Kuba, R. Yamada, G. Ishiguro, R. Adachi, Redistribution of Kv1 and Kv7 enhances neuronal excitability during structural axon initial segment plasticity. *Nat. Commun.* **6**, 8815 (2015).
11. C. Thome *et al.*, Axon-carrying dendrites convey privileged synaptic input in hippocampal neurons. *Neuron* **83**, 1418–1430 (2014).
12. M. S. Hamada, S. Goethals, S. I. de Vries, R. Brette, M. H. P. Kole, Covariation of axon initial segment location and dendritic tree normalizes the somatic action potential. *Proc. Natl. Acad. Sci. U.S.A.* **113**, 14841–14846 (2016).
13. G. Baranauskas, Y. David, I. A. Fleidervish, Spatial mismatch between the Na+ flux and spike initiation in axon initial segment. *Proc. Natl. Acad. Sci. U.S.A.* **110**, 4051–4056 (2013).
14. R. Brette, Sharpness of spike initiation in neurons explained by compartmentalization. *PLoS Comput. Biol.* **9**, e1003338 (2013).
15. S. Goethals, R. Brette, Theoretical relation between axon initial segment geometry and excitability. *eLife* **9**, e53432 (2020).
16. M. Telenczuk, B. Fontaine, R. Brette, The basis of sharp spike onset in standard biophysical models. *PLoS One* **12**, e0175362 (2017).
17. A. T. Gulledge, J. J. Bravo, Neuron morphology influences axon initial segment plasticity. *eNeuro* **3**, ENEURO.0085-15.2016 (2016).
18. S. Goethals, M. C. Sierksma, X. Nicol, A. Réaux-Le Goazigo, R. Brette, Electrical match between initial segment and somatodendritic compartment for action potential backpropagation in retinal ganglion cells. *J. Neurophysiol.* **126**, 28–46 (2021).
19. M. Michalikova, M. W. H. Remme, R. Kempter, Spikelets in pyramidal neurons: Action potentials initiated in the axon initial segment that do not activate the soma. *PLOS Comput. Biol.* **13**, e1005237 (2017).
20. Z. F. Mainen, J. Joerges, J. R. Huguenard, T. J. Sejnowski, A model of spike initiation in neocortical pyramidal neurons. *Neuron* **15**, 1427–1439 (1995).
21. M. H. P. Kole, G. J. Stuart, Is action potential threshold lowest in the axon? *Nat. Neurosci.* **11**, 1253–1255 (2008).
22. J. Hao *et al.*, Kv1.1 channels act as mechanical brake in the senses of touch and pain. *Neuron* **77**, 899–914 (2013).
23. W. Hu *et al.*, Distinct contributions of Na(v)1.6 and Na(v)1.2 in action potential initiation and backpropagation. *Nat. Neurosci.* **12**, 996–1002 (2009).
24. L. M. Palmer, G. J. Stuart, Site of action potential initiation in layer 5 pyramidal neurons. *J. Neurosci.* **26**, 1854–1863 (2006).
25. P. M. Jenkins *et al.*, Giant ankyrin-G: A critical innovation in vertebrate evolution of fast and integrated neuronal signaling. *Proc. Natl. Acad. Sci. U.S.A.* **112**, 957–964 (2015).
26. B. Zonta *et al.*, A critical role for Neurofascin in regulating action potential initiation through maintenance of the axon initial segment. *Neuron* **69**, 945–956 (2011).
27. W. Hu, B. P. Bean, Differential control of axonal and somatic resting potential by voltage-dependent conductances in cortical layer 5 pyramidal neurons. *Neuron* **97**, 1315–1326.e3 (2018).
28. S. Boudkkazi *et al.*, Release-dependent variations in synaptic latency: A putative code for short- and long-term synaptic dynamics. *Neuron* **56**, 1048–1060 (2007).
29. B. Hille, *Ion Channels of Excitable Membranes* (Sinauer Associates, ed. 3, 2001).
30. M. Zbili *et al.*, Axonal Na+ channels detect and transmit levels of input synchrony in local brain circuits. *Sci. Adv.* **6**, eaay4313 (2020).
31. M. Sekerli, C. A. Del Negro, R. H. Lee, R. J. Butera, Estimating action potential thresholds from neuronal time-series: New metrics and evaluation of methodologies. *IEEE Trans. Biomed. Eng.* **51**, 1665–1672 (2004).
32. S. Rama *et al.*, The role of axonal Kv1 channels in CA3 pyramidal cell excitability. *Sci. Rep.* **7**, 315 (2017).
33. J. M. Bekkers, M. Häusser, Targeted dendrotomy reveals active and passive contributions of the dendritic tree to synaptic integration and neuronal output. *Proc. Natl. Acad. Sci. U.S.A.* **104**, 11447–11452 (2007).
34. G. Major, A. U. Larkman, P. Jonas, B. Sakmann, J. J. Jack, Detailed passive cable models of whole-cell recorded CA3 pyramidal neurons in rat hippocampal slices. *J. Neurosci.* **14**, 4613–4638 (1994).
35. H. Alle, J. R. P. Geiger, Combined analog and action potential coding in hippocampal mossy fibers. *Science* **311**, 1290–1293 (2006).
36. D. Golomb *et al.*, Mechanisms of firing patterns in fast-spiking cortical interneurons. *PLoS Comput. Biol.* **3**, e156 (2007).

NEUROSCIENCE